Stress distribution in carbides of spheroidised steel using a polycrystalline modeling

Saeid Rezaee, Clotilde Berdin
Ecole Centrale Paris, L.MSSMat, CNRS UMR 8579, Châtenay-Malabry, France

ABSTRACT

The fracture properties of spheroidised steel, especially the cleavage properties are well known to be related to the carbides damage. Carbides damage has been studied for a long time considering the pile-up of the dislocations against carbide, or from a macroscopic viewpoint, considering the ferrite as an homogeneous isotropic material. In this work the ferrite is modeled at the crystalline level.
The microstructure generation is performed through a finite element method: a crystalline model is used for the grains behavior modeled by hexagons or Voronoï Tesselation. The carbides are modeled in the form of spherical particles and are randomly located within the ferrite grains. The stress distribution in the carbides is studied considering the different random crystalline orientation of the grains. The effect of the carbide size relative to the grain size, and the influence of the grains morphology on the carbide loading are presented as well.

1 INTRODUCTION

The single parameter (global) and the micro-mechanical local based fracture mechanical approaches are limited in describing the fracture of ferritic steels especially in the ductile to brittle transition (DBT) domain. In this domain, the both type of fracture are activated: brittle fracture is preceded by initiation and propagation of a ductile tearing. The brittle fracture can be studied in the lower shelf of DBT by the local approaches developed by Ritchie et al. (RKR model) or by Beremin. The Gurson model modified by Needleman and Tvergaard (GTN model) can be used to predict the ductile fracture in the higher shelf of DBT range. Bernauer et al. [1], Rossoll et al. [2] and Haušild et al. [3] coupled the Beremin and GTN model and Tanguy et al. [4] coupled the Rousselier and Beremin model to describe the fracture in the DBT domain. These studies showed that the parameters of the Beremin model have to be changed with temperature to account for the sharp increase in toughness with the temperature for bainitic steels.
These results were explained by the evolution of the distribution of defects triggering cleavage. However, no clear evidence of that statement was showed. Indeed, there are many micro-structural features like bainitic lath width, packet size and prior austenitic grain size in bainitic steels [3] that are evoked as critical feature for cleavage in these steels.
So in this study, we propose to investigate the influence of crystalline scale on cleavage fracture initiation of an idealized steel with brittle particles, like a spheroidized steel. Indeed in this type of steel, the cleavage fracture has been investigated for a long time, and there are only the grain size and the carbide size that have a role on the fracture [5]. The crystallographic orientation of the ferrite

grain is considered through a crystalline model based on the continuous theory of dislocation. The carbides are modeled in spherical form in the ferrite using an isotropic elastic behavior. Stress distribution in the carbide is studied by varying different parameters: local crystallographic orientation, relative size of the grains and carbides, spatial distribution of carbides and morphology of the grain.

2 POLYCRYSTALLINE MODEL AND NUMERICAL PROCEDURE

2.1 Polycrystalline model

The model Cristal-ECP developed in the MSSMat laboratory of Ecole Centrale Paris is used in this study [6]. This model takes into account the plastic slip on the different slip systems. The model is based on the dislocation theory, using the mean dislocation density on the slip systems. The viscoplastic glide on the slip system s is activated when the Schmid's criterion is satisfied, *i.e.* when the shear stress on the slip system s, τ^s reaches a critical value τ_c^s. The viscoplastic flow rule is a power law that can be used for both B.C.C. and F.C.C. structure materials:

$$\dot{\gamma}^s = \dot{\gamma}_0^s \left(\frac{\tau^s}{\tau_c^s} \right)^n \quad \text{if } \left| \tau^s \right| \geq \tau_c^s \tag{2.1}$$

where $\dot{\gamma}_0^s$ is a reference strain rate and n is the rate sensibility exponent. The critical shear stress on the slip system s can be related to the dislocation density on each slip system:

$$\tau_c^s = \tau_0 + \mu b \sqrt{\sum_u a^{su} \rho^u} \tag{2.2}$$

where a^{su} introduces the dislocation interaction between different slip systems s and u, τ_0 is a temperature dependant friction stress, μ is the shear modulus, and ρ^u is the dislocation density on the activated slip system u. The dislocation density evolution law is derived by considering two main terms associated with dislocation creation and dislocation annihilation:

$$\dot{\rho}^s = \frac{\left| \dot{\gamma}^s \right|}{b} \left(\frac{\sqrt{\sum_{u \neq s} \rho^u}}{K} - 2 y_c \rho^s \right) \tag{2.3}$$

where K is the number of obstacles which has been passed over by the dislocations, y_c is a characteristic distance of dislocation annihilation and b is the Burger's vector. The hardening law relates the critical shear stress rate on the slip system s to the cumulated glide rate of all the systems, by introducing a hardening matrix h^{su}. The diagonal components of h^{su} correspond to the auto-hardening and the off-diagonal components represent the cross-hardening effect. Using the equations the hardening matrix h^{su} can be represented as:

$$h^{su} = \frac{\mu a^{su}}{2} \frac{1}{\sqrt{\sum_t a^{st} \rho^t}} \left(\frac{\sqrt{\sum_{t \neq s} \rho^t}}{K} - 2 \frac{y_c}{b} \rho^u \right) \tag{2.4}$$

2.2 Microstructure generation

In the first step of study, the microstructure is constructed with hexagons representing the grains of ferrite and circles representing the carbides. This 2D-representation is extended in the third direction by translation. The ratio of the grain to carbide size is fixed to 5 and the volume fraction of the carbides is fixed to 5%. The carbides are randomly located in the microstructure. In the second step, the grains are generated by a random tessellation method: the Voronoï polyhedra The grain to carbide size ratio reaches approximately 5 by a minimum distance prescribed between the centers of the polyhedra.

The Young modulus E for cementite is reported between 170 GPa and 269 GPa in the literature [7,8]. An intermediate value of 210 GPa is set for the Young modulus. The Poisson ratio v is set to 0.3 [7, 8].

For the crystalline model, 12 coefficients have to be determined. The elastic behaviour at crystalline scale is defined by the rigidity tensor C which uses 3 independent coefficients C_{11}, C_{12} and C_{44}. In the case of isotropy this tensor can be defined by 2 coefficients E and υ. The crystalline behaviour parameters of IF-Ti steel were identified by Erieau [6] and they were used in this work (Table 1). This is a ferritic steel and its low inclusion content lets us to use its parameters to represent the behaviour of a ferritic matrix. It should be noted that these parameters were obtained at room temperature, so this study is only a parametric study and not a prediction to cleavage fracture.

Table 1 : Crystalline material behaviour parameters [6]

E (GPa)	v	n	$\dot{\gamma}_0$ (s^{-1})	τ_0 (MPa)	b (nm)
210	0.29	100	10^{-11}	20	0.25
P_0 (m^{-2})	a^{ss}	a^{su}	g_c (nm)	K	D (mm)
15×10^{9}	0.25	0.25	8	41	0.075

The different crystalline orientations are defined by Bunges's Euler angles (φ_1, ϕ, φ_2), referring to the three rotations which transform the global coordinate system into the crystal coordinate system. The grain orientations are randomly distributed considering that $0^\circ \le \varphi_1, \varphi_2 \le 360^\circ$ and $-1 \le \cos\phi \le 1$. The {001} and {011} pole figures presented in Figure 1 show an isotropic distribution of crystalline orientations for 117 grains.

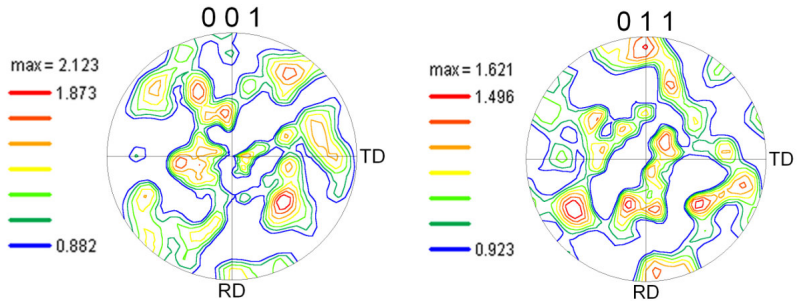

Figure 1 : {001} and {011} pole figures obtained by random generation of 117 grains.

2.3 Finite element modelling

The polycrystalline model has been implemented in the *ABAQUS* finite element code (using *UMAT* subroutine) in the large transformation framework. The constitutive equations are integrated by an explicit forward gradient procedure.
The microstructure is generated in 2D but an extension in the third direction perpendicular to the grain boundaries is performed to allow the glide on any slip systems. The 3D elements of type C3D8R (linear 8-nodes bricks, reduced integration, hourglass controlled element) were used. Three layers were modeled. Figure 2 and Figure 3 show two types of microstructure generated by the hexagons and the Voronoï polyhedras. In the Figure 2(b) the carbides are located at the grains boundaries, which is a better modeling of spheroidal steel. Each color represents one crystalline orientation. The carbides are shown by the black circles:

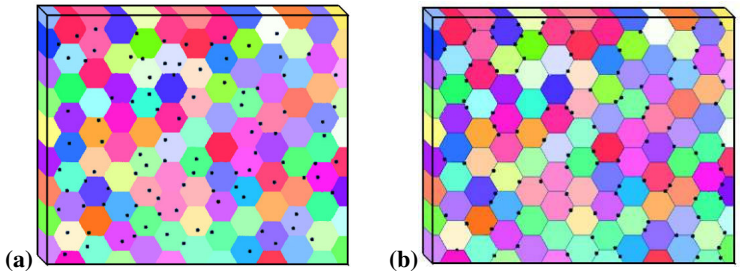

Figure 2 : Microstructure representation by hexagons (a) carbides in the microstructure (b) carbides in the grains boundaries

Two types of boundary conditions have been studied: 1) global plane deformation condition has been imposed by blocking the both faces of the model in the third direction in order to approximate the mechanical state as ahead of a crack tip in a thick specimen; 2) plane stress analyses by blocking one face in third direction and prescribing an homogeneous displacement in the third direction on other external faces. Homogeneous displacement condition in direction 1 was imposed for the lateral faces in the plane of the microstructure ($U_1 = U_{10}^*$). The displacement in direction 2 was blocked on the bottom face and a displacement of 10% in height is imposed on the top face (Figure 3(b)).

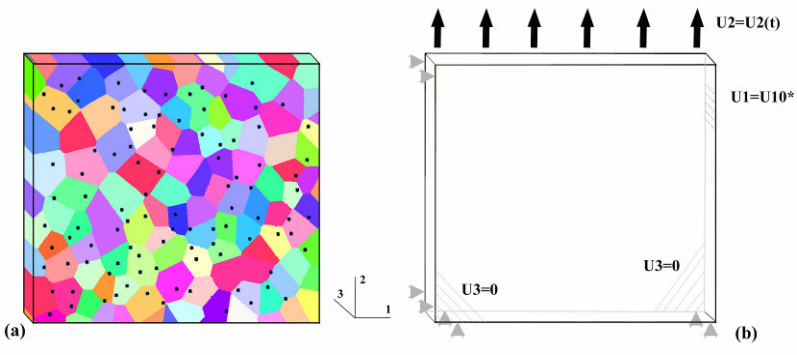

Figure 3 : (a) Microstructure representation by Voronoï polyhedras (b) Boundary conditions.

The strain rate is set to 10^{-4} /s and all finite element results are obtained from the analysis of the middle layer to prevent some boundary effects on the results.

3 RESULTS AND DISCUSSION

3.1 Crystalline heterogeneity influence

The finite element results show a strong heterogeneity in the stress and strain fields (Figure 4). The strain in the extension direction reaches locally 42%. These large values are essentially located at the grains boundaries and sometimes at the carbide-grain interfaces. Whereas the strain localised in 45° bands from the traction axis, the traction stress isocontours form paths parallel to the traction axis (σ_{22}). The stress concentrations are located at the grains boundaries or in the carbides. The concentrations at the grains boundaries are due to the adjacent grain misorientation and the concentration at the carbide/ferrite interface is due to the different material behaviour.

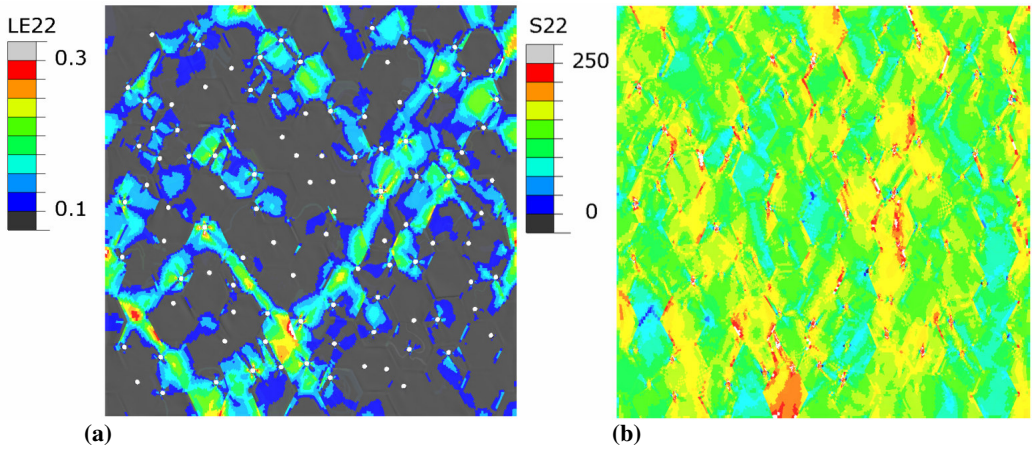

Figure 4 : (a) Strain distribution in the traction direction (b) Traction stress distribution

After 10% of deformation, the largest values of the traction stress in the grains is almost twofold the mean value of the layer ($<\sigma_{22}>_{layer}$), and the largest ones in the carbides are threefold this mean value.

The computation considering an homogeneous equivalent material for the grains is performed in plane stress condition, in order to study the influence of the local crystalline behaviour on the mechanical fields. This material behaviour is obtained by the stress-strain global curve in a plane stress crystalline analysis, and is considered as isotropic elastic-plastic behaviour. The heterogeneity of the mechanical fields (stress and strain) is very low.

The mean traction stress in the carbide and the coefficient of variation (C_v, the standard deviation divided by the mean value in the layer) are plotted versus deformation in the Figure 5(a) and 5(b). Considering the matrix as polycrystalline medium leads to a higher variation coefficient that is twofold the one in homogeneous computation at 10% of macroscopic strain. This last point is important for statistics of fracture: the mean macroscopic fracture stress predicted

by a polycrystalline approach could be lower than the mean fracture stress predicted by a homogeneous approach. The strain level modifies the mean stress in the particles at is will be expected. But, whereas, the carbide mean stress to the layer mean stress in polycrystalline simulation increases with the increase of the macroscopic strain, it decreases in the homogeneous simulation: in homogeneous simulations the stress in the layer increases more rapidly than the stress in the carbides, whereas in polycrystalline simulations the difference between carbides and matrix (grains) stress increases with macroscopic strain.

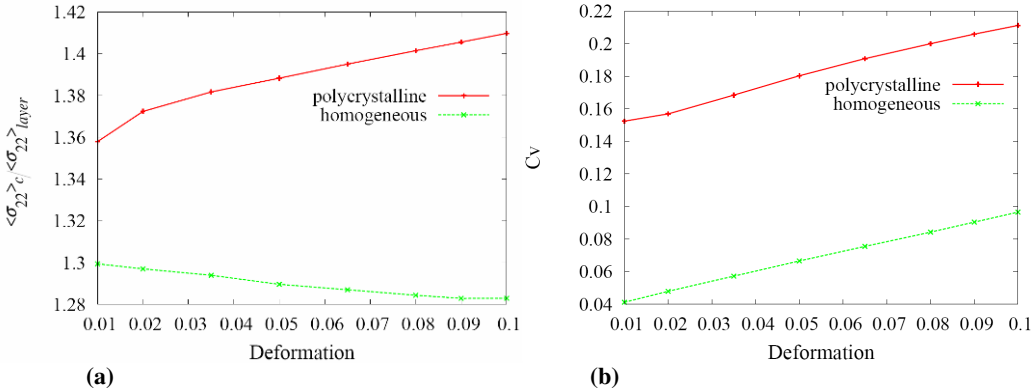

Figure 5 : (a) Carbide mean stress divided by layer mean stress (b) coefficient of variation (C_v), versus deformation in polycrystalline and homogeneous simulations

The stress distribution within the carbides is reported (Figures 6) and confirms the results discussed above. However, the distribution is asymmetric for the low values of macroscopic strain: the modal value is lower than the mean value (Figure 6(b)). This skewness diminishes as the macroscopic strain increases.
So, considering that the elastic particles are embedded in a polycrystalline matrix rather than in an homogeneous material, leads to a higher stress computed in the particles, and a higher scatter.

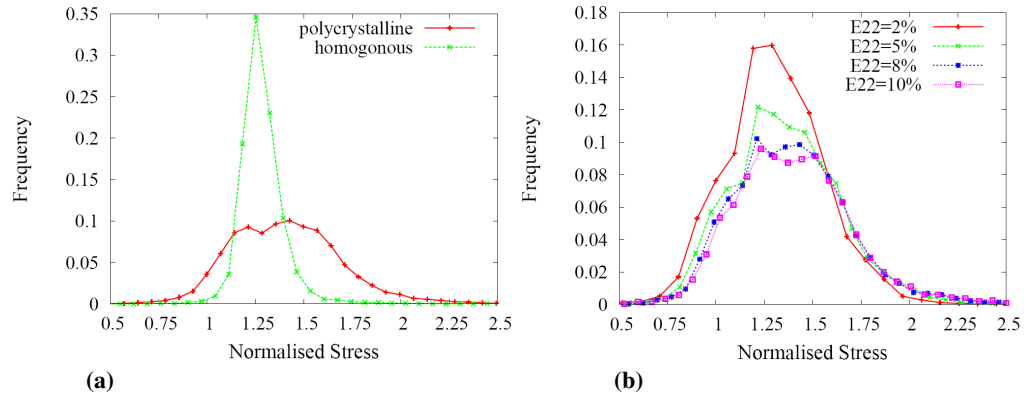

Figure 6 : Carbide stress distribution (a) for polycrystalline simulations and homogeneous simulations in plane stress (b) for different level of deformation in polycrystalline plane strain simulation

3.2 Influence of crystalline orientations

In order to study the influence of the local crystalline orientation on the global behaviour and on the local stress distribution, three calculations were performed using three different crystalline orientation distributions. The coefficient of variation shows only a 8% difference between the three simulations and mean stress in the carbide do not show a large change (Figure 7). The strain and stress fields are globally similar in the three analyses. However, local stress distribution within a carbide is sensitive to the different orientations of the surrounding grains. So, further investigations of this local influence were performed. One of the carbides subjected to a high stress level is chosen. The chosen carbide is located in the grain that presents a high level of deformation. The orientations of the grain containing the carbide and the six surrounding grains were changed. The carbide containing grain's deformation field shows a 37% decrease in its mean value (Figure 8). The mean value of the carbide stress decreases down to 20% (Figure 9).

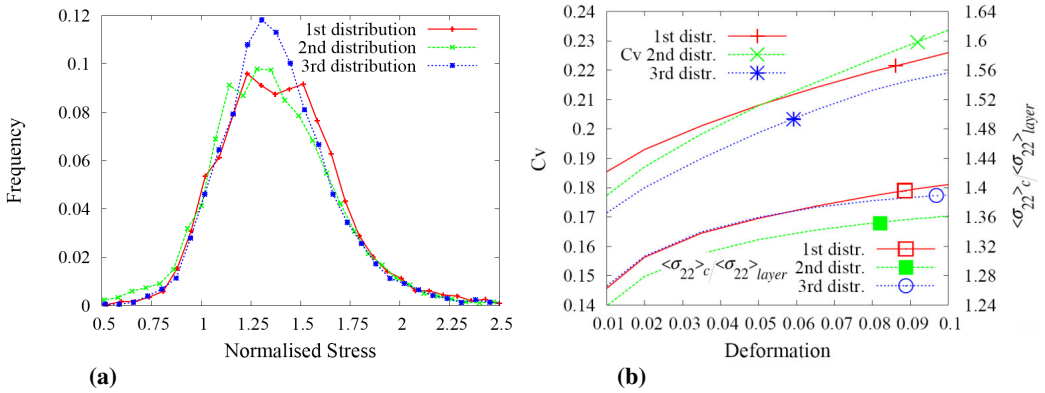

Figure 7 : (a) Carbide stress distribution (b) Coefficients of variation (C_v) and Carbide mean stress divided by layer mean stress, for 3 distributions

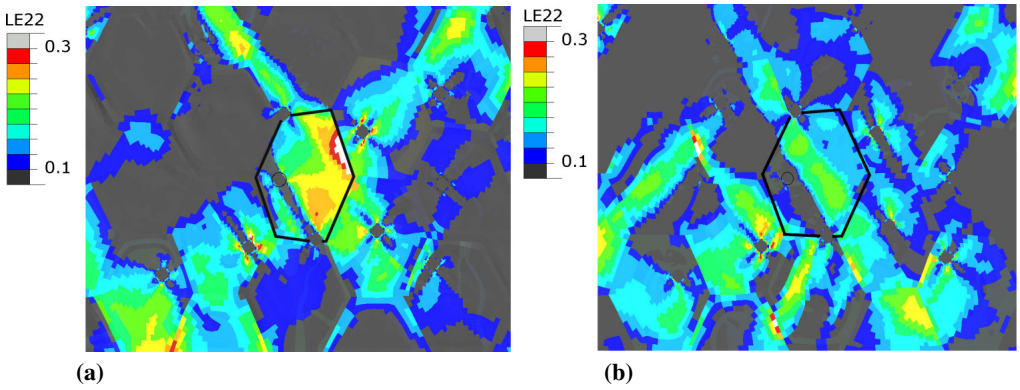

Figure 8 : Strain isocontour in the traction direction (a) for the initial distribution (b) after changing the surrounding grains orientations

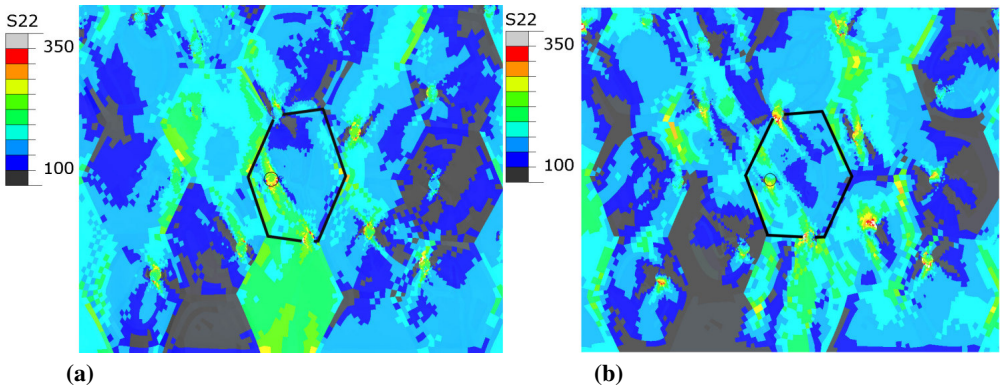

Figure 9 : Traction stress isocontour (a) for the initial distribution (b) after changing the surrounding grains orientations

3.3 Influence of the carbides spatial distribution

The carbide spatial distribution is modified by a new random generation in the initial crystallographic orientation of hexagonal cells. The nearest neighbourhood distance shows that the first spatial distribution is less homogeneous than the second one (Figure 10(a)) but the stress distributions within the carbides are almost similar, except a shift in mean value towards the higher values for the first spatial distribution. However, this difference is small and the elementary volume can be considered as representative from this viewpoint.

The finite element analyses show that the critical carbide can be located in the grain or at the grain boundary and both positions could be critical. So the carbides are located only at the grains boundaries to study its influence on the carbide stress distribution. The nearest neighbourhood distance shows an inhomogeneous distribution. It means that the carbides are located either close together or at a large distance. So, the stress scatter in this case is more important. This can be observed from the carbide stress distribution (Figure 10(b)). It should be noted that the global stress-strain curves and the stress and strain fields are not sensitive to the location of the carbides.

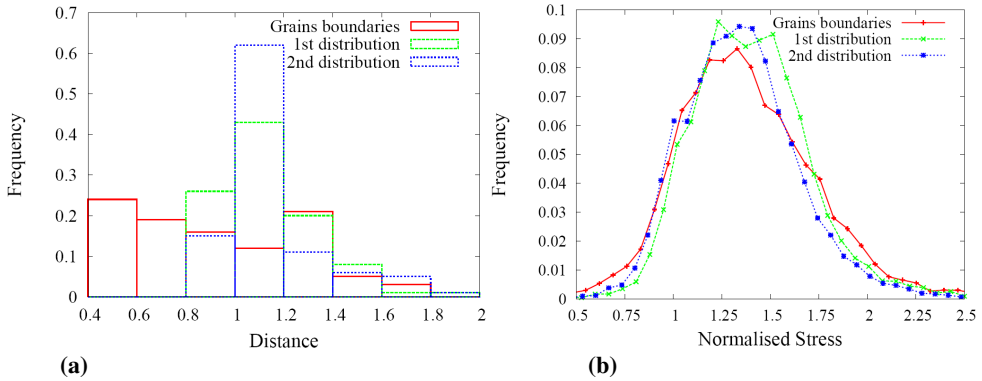

Figure 10 : (a) The carbides nearest neighbourhood distance distribution (b) Carbides stress distribution regarding to two different carbide spatial distributions and the grains boundary carbides

3.4 Influence of grain morphology and carbides size

A traction transverse to the first direction was carried out. The carbides stress dispersion and the mean stress in the carbides are almost identical. The scatter in carbide stress distribution is lower than the scatter obtained by a traction in the vertical direction (Figure 11(b)).
The influence of grain morphology is studied using the Voronoï tessellation to model the grains instead of hexagonal cells. The traction stress isocontours is more heterogeneous and high values are located at the grains boundaries. The stress histograms and the global properties do not change, but the carbides stresses are influenced individually.
A simulation is performed using the initial crystallographic orientation distribution and carbides spatial distribution, except that the size of the carbides is increased by a factor 2. The carbide stress histograms do not show an important difference and the stress and the strain in the grains are almost same. The locations of the critical carbides, i.e. the carbides submitted to a high value of stress remains the same (Figure 11).

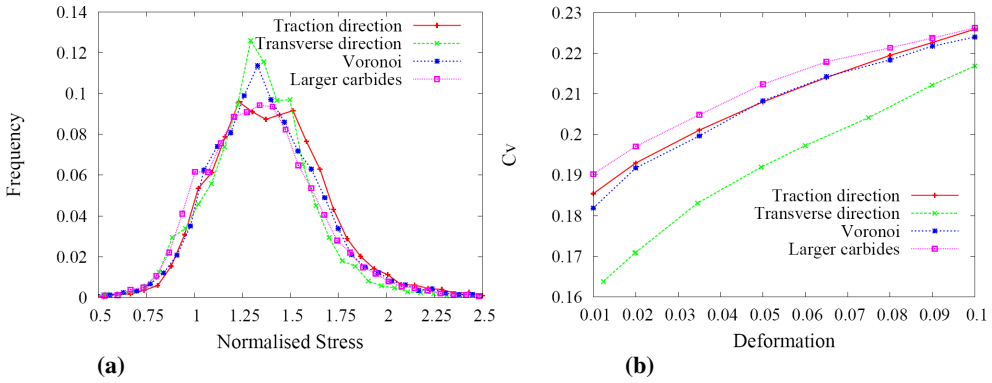

Figure 11 : (a) Carbide stress distribution (b) Coefficient of variation (C_v), for simulations in traction and tranverse direction, and with Voronoi tessellation and larger carbides

4 CONCLUSION

The polycrystalline and homogeneous simulations results shows that the mechanical field heterogeneity in the grains and carbides can not be modeled by the homogeneous simulation and it is necessary to use polycrystalline simulation to study the stress distribution in the carbides. It is shown that the global behaviour of the microstructure does not change by changing the orientation distribution. The results are not sensitive to the spatial distribution of the carbides for the volume fraction studied. It means that the results are independent of the grain orientations distribution and the microstructure can be considered as a representative elementary volume. Nevertheless, this conclusion should be confirmed by a larger number of simulations.
The stress level in the carbides are related to the surrounding grains crystallographic orientation. It is not influenced by the grain morphology and the hexagonal cell is not a critical assumption from this viewpoint. The carbides that

are highly loaded can be located within the grain or at the grain boundary. Considering that the particles are only at the grain boundaries for a given volume fraction leads to an increase of the scatter of the carbide stress. Nevertheless, this influence is mainly induced by the neighbour distance distribution which is very large, in comparison with those obtained for the assumption of the carbide located in the volume.

The mean stress in the carbide relative to the macroscopic stress increases with macroscopic strain, but the scatter increases too. These distributions would be used in probabilistic approaches to the cleavage fracture driven by the particle fracture.

REFERENCES

[1] G. Bernauer, W. Brocks, W. Schmitt, Modifications of the Beremin model for cleavage fracture in the transition region of a ferritic steel, Engineering Fracture Mechanics 64 (1999), 305-325.

[2] A. Rossoll, C. Berdin, C. Prioul, Determination of the fracture toughness of a low alloy steel by the instrumented Charpy impact test, International Journal of Fracture 115 (2002), 205-226.

[3] P. Haušild, C. Berdin, P. Bompard, Prediction of cleavage fracture for a low-alloy steel in the ductile-to-brittle transition temperature range, Materials Science and Engineering A 39 (2005), 188–197.

[4] B. Tanguy, J. Besson, R. Piques, A. Pineau, Ductile to brittle transition of an A508 steel characterized by Charpy impact test Part II: modeling of the Charpy transition curve, Engineering Fracture Mechanics 72 (2005), 413–434.

[5] D.A. Curry, J.F. Knott, Effect of microstructure on cleavage fracture stress in steels, Metal Science, (1978), 511-514.

[6] P. Erieau, C. Rey, Modeling of deformation and rotation bands and of deformation induced grain boundaries in IF steel aggregate during large plane strain compression, International Journal of Plasticity 20 (2004), 1763–1788.

[7] H. Mizubayashi, S.J. Li, H. Yumoto, M. Shimotomai, Young's modulus of single phase cementite, Scripta Materialia, 40 (7) (1999), 773–777.

[8] L. Che, M. Gotoh, Y. Horimoto, Y. Hirose, L. Yang, Characterization of Deformability of Spheroidal Cementite by Residual Stress Measurement, Journal of Materials Engineering and Performance Volume 17(3) (2008), 445-453.